Supporting Information

AAg$_2$PS$_4$ (A = K, Na/K): the first-type of noncentrosymmetric alkali metal Ag-based thiophosphates exhibiting excellent second-order nonlinear optical performances

Wenfeng Zhou,[a] Bingxuan Li,[b] Wenlong Liu,[a] and Sheng-Ping Guo*[a]

[a] *School of Chemistry and Chemical Engineering, Yangzhou University, Yangzhou, Jiangsu 225002, P. R. China*

[b] *Key Laboratory of Optoelectronic Materials Chemistry and Physics, Fujian Institute of Research on the Structure of Matter, Chinese Academy of Sciences, Fuzhou, Fujian 350002, China*

Corresponding author: spguo@yzu.edu.cn

Supplementary Information Index

Tables and Figures

Table S1. Crystal data and structure refinement parameters for **1** and **2**.

Empirical formula	KAg_2PS_4 (**1**)	$(Na_{0.30}K_{0.70})Ag_2PS_4$ (**2**)
Formula weight	414.05	409.30
Temperature/K	293(2)	293(2)
Crystal system	Tetragonal	Tetragonal
Space group	$I\bar{4}2m$	$I\bar{4}2m$
a/Å	6.5985(3)	6.5992(3)
c/Å	8.1549(9)	8.1499(6)
V/Å^3	355.07(5)	354.92(5)
Z	2	2
D_{calc} g/cm^3	3.873	3.830
μ/mm^{-1}	7.383	7.231
F(000)	384.0	379.0
2θ range for data collection/°	7.994 to 54.984	7.946 to 60.264
Index ranges	$-8 \leq h \leq 5$, $-8 \leq k \leq 7$, $-10 \leq l \leq 10$	$-9 \leq h \leq 6$, $-6 \leq k \leq 9$, $-11 \leq l \leq 11$
Reflections collected	852	932
Independent reflections	220 [R_{int} = 0.0230, R_{σ} = 0.0220]	280 [R_{int} = 0.02301, R_{σ} = 0.0227]
Data/restraints/parameters	220/0/14	280/0/15
Goodness-of-fit on F^2	1.065	1.058
Flack parameter	0.04 (3)	0.00 (3)
Final R indexes [I $\geq 2\sigma$ (I)]	R1 = 0.0238, wR2 = 0.0666	R1 = 0.0223, wR2 = 0.0699
Final R indexes [all data]	R1 = 0.0241, wR2 = 0.0669	R1 = 0.0225, wR2 = 0.0700
Largest diff. peak/hole/e Å^{-3}	0.79/-0.67	0.50/-0.68

[a]$R1 = ||F_o| - |F_c||/|F_o|$. [b]$wR2 = [w(F_o^2 - F_c^2)^2]/[w(F_o^2)^2]^{1/2}$.

Table S2. Atomic coordinates ($\times 10^4$) and equivalent isotropic displacement parameters ($\text{Å}^2 \times 10^3$) for **1** and **2**. U_{eq} is defined as 1/3 of the trace of the orthogonalized U_{ij} tensor.

Atom	Wyckoff site	x	y	z	U_{eq}
			1		
K	2*a*	5000	5000	5000	25.9(8)
Ag	4*d*	0	5000	2500	40.8(6)
P	2*b*	0	10000	5000	8.9(7)
S	8*i*	1819(2)	8181(2)	3602(2)	18.1(6)
			2		
Na/K	2*a*	5000	5000	5000	27.7(16)
Ag	4*d*	5000	10000	7500	39.6(4)
P	2*b*	0	10000	5000	11.4(5)
S	8*i*	1822.9(18)	8177.1(18)	6393.1(18)	21.5(5)

Table S3. Bond lengths (Å) for **1**.

Bond	Length/Å	Bond	Length/Å
	1		**2**
K(1)–S(1)	3.180(2) × 4	Na(1)/K(1)–S(1)	3.175(2) × 4
Ag(1)–S(1)	2.580(8) × 4	Ag(1)–S(1)	2.580(6) × 4
P(1)–S(1)	2.044(2) × 4	P(1)–S(1)	2.045(2) × 4

Table S4. The EDS results of **1** and **2**.

Molar ratio	Na	K	Ag	P	S
1	–	10.15	21.21	15.69	52.95
2	3.89	9.18	20.79	13.82	52.33

Table S5. Bond valence sums **1** and **2**.

Atoms	BVS	Atoms	BVS
	1		**2**
K	0.90	Na/K	0.73
Ag	1.15	Ag	1.15
P	4.89	P	4.90
S	-2.02	S	-1.95

Table S6. The calculated dipole moment and distortion ($\sigma_{\theta(\text{tet})}^2$) of single AgS_4 tetrahedron among **1** and the known Ag-based thiophosphates.

Compound	Magnitude (deby)	$\sigma_{\theta(\text{tet})}^2$	Compound	magnitude (deby)	$\sigma_{\theta(\text{tet})}^2$
1	13.43	474.9	$AgHgPS_4$	9.29	14.85
Ag_3PS_4	4.76	20.54	$AgHg_3PS_6$	8.36	73.42
$AgZnPS_4$	7.40	18.23	$AgCd_3PS_6$	4.28	159.4

Note: $\sigma_{\theta(\text{tet})}^2 = \dfrac{\sum_{i=1}^{6}(\theta_t - 109.47^\circ)}{5}$, where $\sigma_{\theta(\text{tet})}^2$ is used to describe the distortion and θ_t is the bond angle.

Table S7. The NLO data of known NLO-active thiophosphates with 3D framework.

Compound	Space group	Structural units	Band gap (eV)	SHG	LIDT	PM/ NPM	Ref.
Ag_3PS_4	$Pmn2_1$	AgS_4, PS_4	2.43	1.3 × AGS	–	PM	[1]
Cu_3PS_4	$Pmn2_1$	CuS_4, PS_4	2.25	0.5 × AGS	–	NPM	[1]
$Ag_{1.5}Cu_{1.5}PS_4$	$Pmn2_1$	$(Ag/Cu)S_4$, PS_4	2.37	0.8 × AGS	–	PM	[1]
$Eu_2P_2S_6$	Pn	EuS_8, P_2S_6	2.54	0.9 × AGS	3.4 × AGS	PM	[2]
$Ba_2P_2S_6$	Pn	BaS_6, P_2S_6	4.3	1.7 × AGS	5.5 × AGS	NPM	[3]
$Pb_2P_2S_6$	Pn	PbS_6, P_2S_6	2.6	1.4 × AGS	2.5 × AGS	PM	[3]
$Zn_3P_2S_8$	$P\bar{4}n2$	ZnS_4, PS_4	3.12	2.6 × AGS	–	PM	[4]
$Hg_3P_2S_8$	$Aea2$	HgS_4, PS_4	2.77	4.2 × AGS	4 × AGS	PM	[5]
$SnPS_3$	Pn	SnS_8, P_2S_6	2.35	1.1 × AGS	6.9 × AGS	PM	[6]
KAg_2PS_4	$I\bar{4}2m$	AgS_4, PS_4	2.92	1.40 × AGS	3.49 × AGS	PM	This work
$(Na_{0.30}K_{0.70})Ag_2PS_4$	$I\bar{4}2m$	AgS_4, PS_4	2.89	1.65 × AGS	2.77 × AGS	PM	This work
$AgZnPS_4$	$Pna2_1$	AgS_4, ZnS_4, PS_4	2.76	1.8 × AGS	–	PM	[7]
$CuZnPS_4$	$I\bar{4}2m$	CuS_4, ZnS_4, PS_4	3.00	3 × AGS	6 × AGS	PM	[8]
$LiZnPS_4$	$I\bar{4}$	LiS_4, ZnS_4, PS_4	3.38	0.8 × AGS	–	PM	[7]
$Cu_5Zn_{0.5}P_2S_8$	$Pmn2_1$	$(Cu/Zn)S_4$, ZnS_4, PS_4	2.31	0.3 × AGS	3.2 × AGS	PM	[9]
$AgHgPS_4$	Pn	AgS_4, HgS_4, PS_4	2.63	5.09 × AGS	–	PM	[10]
$CuHgPS_4$	$Pna2_1$	CuS_4, HgS_4, PS_4	2.03	6.5 × AGS	4.2 × AGS	PM	[11]
$NaHgPS_4$	$P\bar{4}n2$	HgS_4, PS_4	2.78	3.14 × AGS	–	PM	[12]
$KHgPS_4$	$Pnn2$	HgS_4, PS_4	2.90	4.15 × AGS	–	PM	[12]
$AgHg_3PS_6$	Cc	AgS_4, HgS_4, PS_4	1.85	0.5 × AGS	–	NPM	[13]
$Cu_5Hg_{0.5}P_2S_8$	$Pmn2_1$	CuS_4, HgS_4, PS_4	2.12	0.8 × AGS	–	PM	[13]
$AgCd_3PS_6$	Cc	AgS_4, CdS_4, PS_4	2.56	0.45 × AGS	–	–	[14]
$CuCd_3PS_6$	Cc	CuS_4, CdS_4, PS_4	2.24	0.9× AGS	4.1 × AGS	NPM	[15]
$LiCd_3PS_6$	Cc	LiS_4, CdS_4, PS_4	2.97	0.8 × AGS	5.5 × AGS	PM	[16]
$AgGa_2PS_6$	Cc	AgS_3, GaS_4, PS_4	2.75	1 × AGS	5.1 × AGS	PM	[17]
$LiGa_2PS_6$	Cc	LiS_4, GaS_4, PS_4	3.15	0.5 × AGS	10.4 × AGS	–	[16]

$KSbP_2S_6$	$Pna2_1$	KS_9, SbS_7, P_2S_6	2.9	$2.2 \times AGS$	$3 \times AGS$	PM	[18]
$KBiP_2S_6$	$Pna2_1$	KS_9, BiS_7, P_2S_6	2.3	$1.8 \times AGS$	$3 \times AGS$	PM	[18]
$K_2BaP_2S_6$	$Pna2_1$	KS_7,KS_8, BaS_{10}, P_2S_6	4.1	$2.1 \times AGS$	$8 \times AGS$	PM	[18]
$RbBiP_2S_6$	$P2_1$	BiS_7, P_2S_6	2.10	$11.9 \times AGS$	$11.3 \times AGS$	PM	[19]

Table S8. The measured birefringence of **2** at the wavelength of 546.1 nm with polarizing microscope.

Crystal	Retardation (ΔR, μm)	Thickness (μm)	Birefringence (Δn)
2	1.618	6.7	0.24
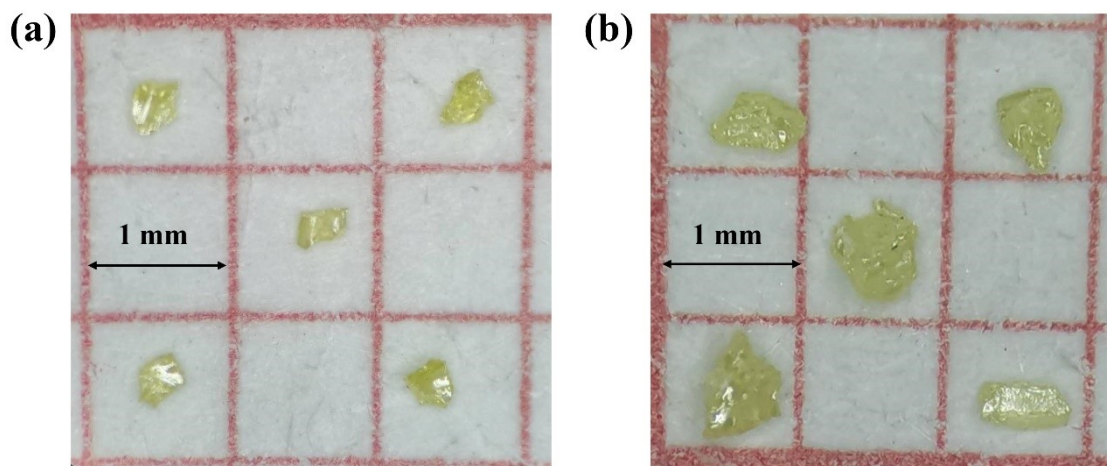
Fig. S1. Photographs of the crystals for (a) **1** and (b) **2**.
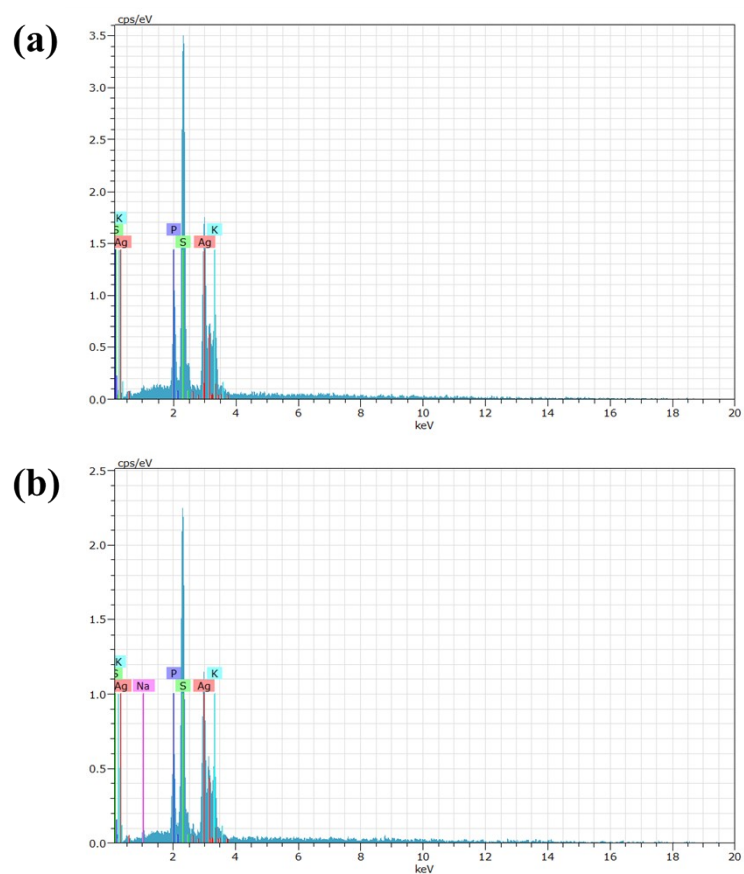

Fig. S2. The EDS images for single crystals of (a) **1** and (b) **2**.
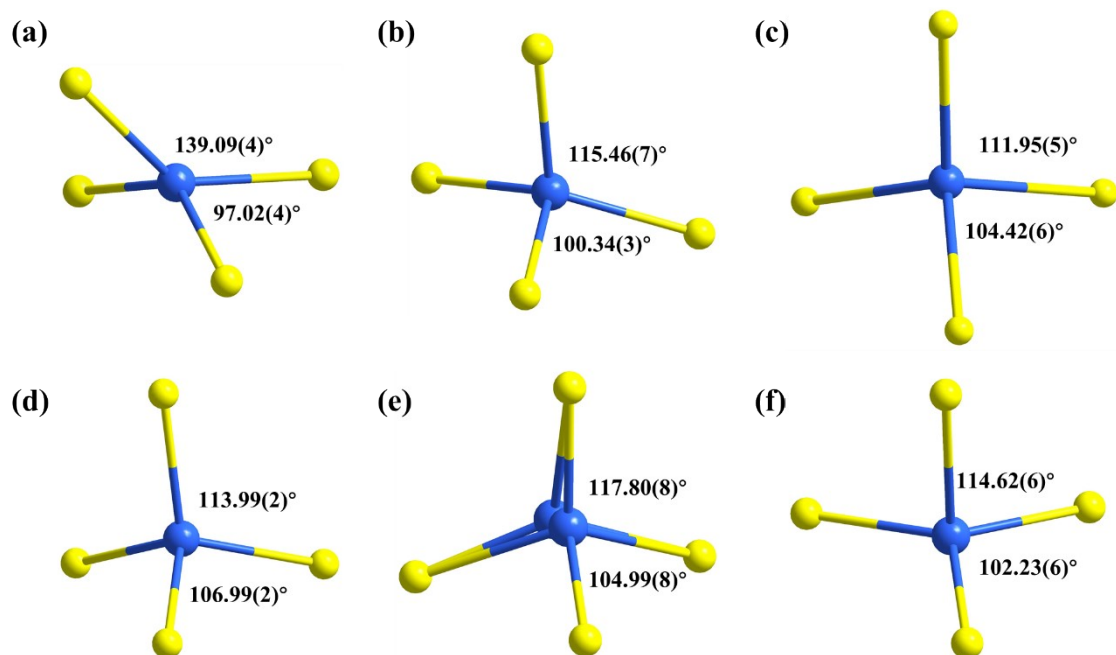
Fig. S3. AgS_4 tetrahedra in (a) **1**, (b) Ag_3PS_4, (c) $AgZnPS_4$, (d) $AgHgPS_4$, (e) $AgHg_3PS_6$, and (f) $AgCd_3PS_6$.
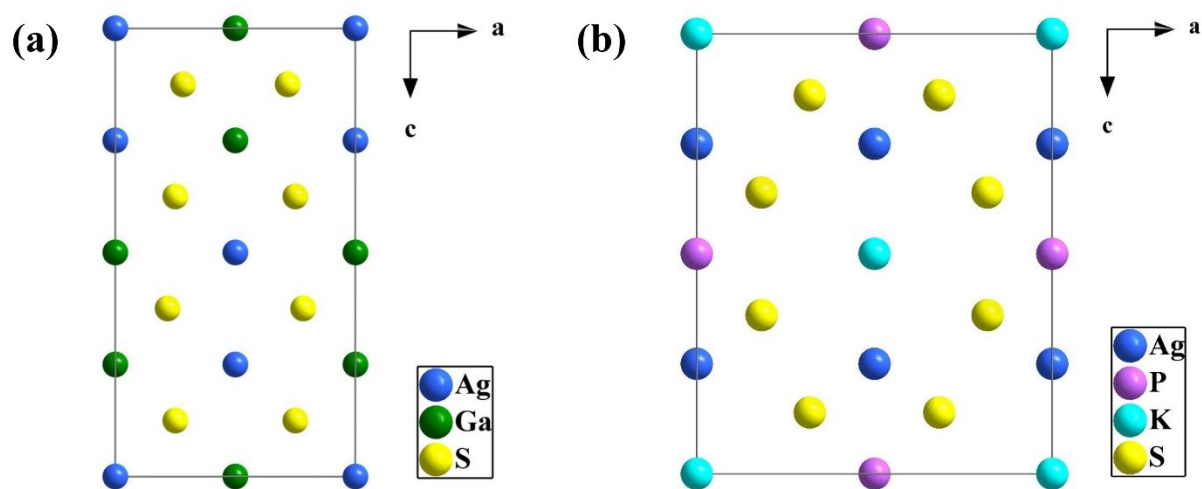

$$2Ag^+ + 2Ga^{3+} \rightarrow K^+/Na^+ + 2Ag^+ + P^{5+}$$

Fig. S4. Structural evolution from (a) AGS to (b) **1**.
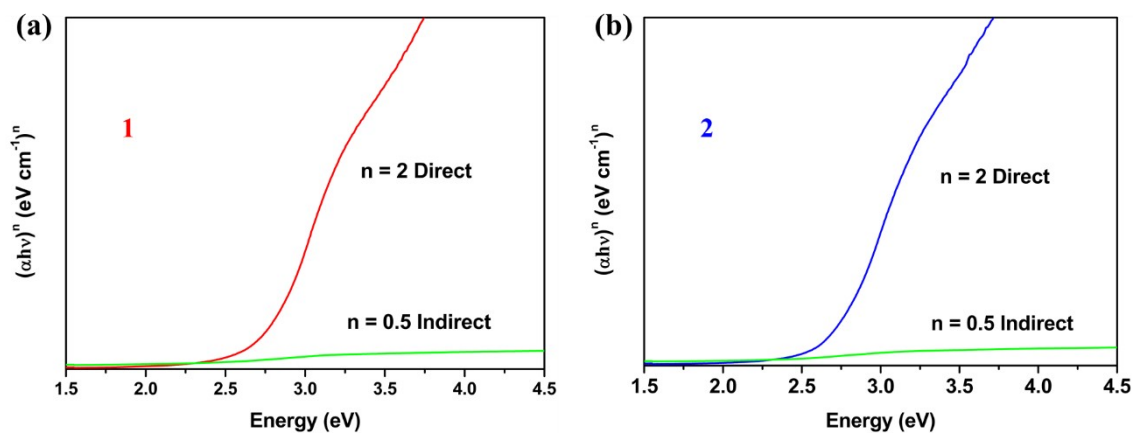
Fig. S5. Tauc plots of **1** and **2**. n = 2 (red and blue lines): direct band gap; n = 1/2 (green lines): indirect band gap.
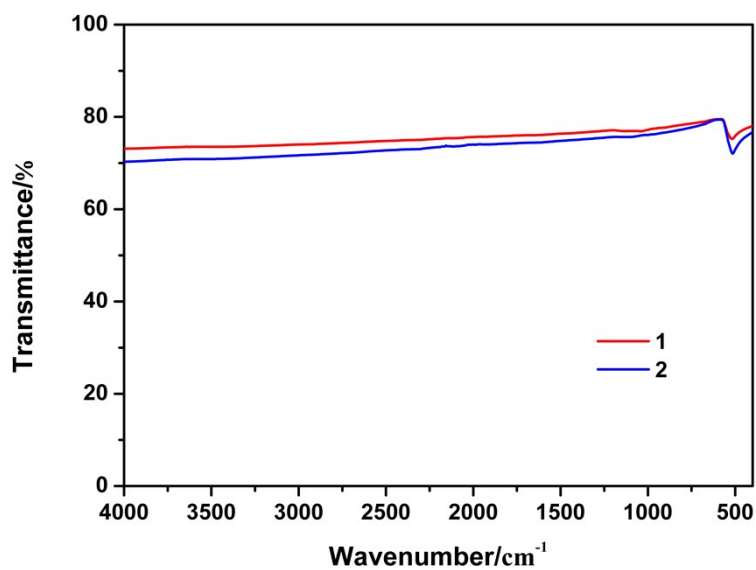

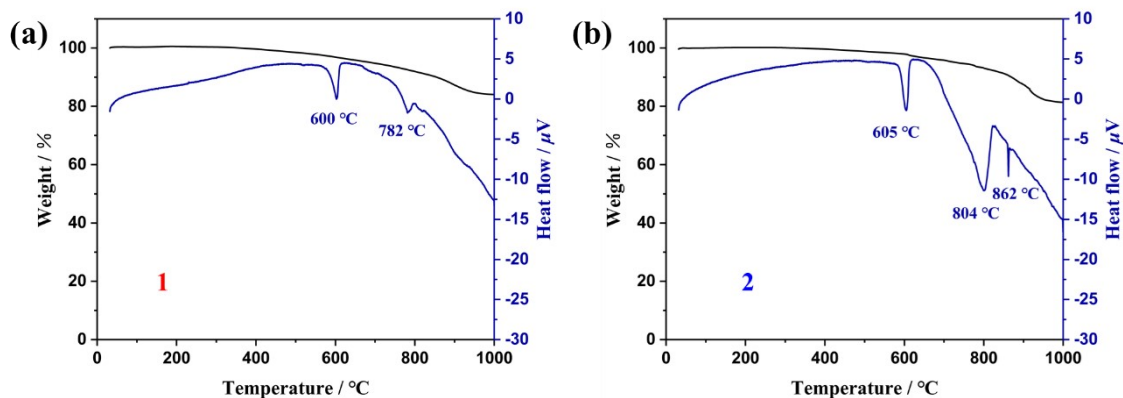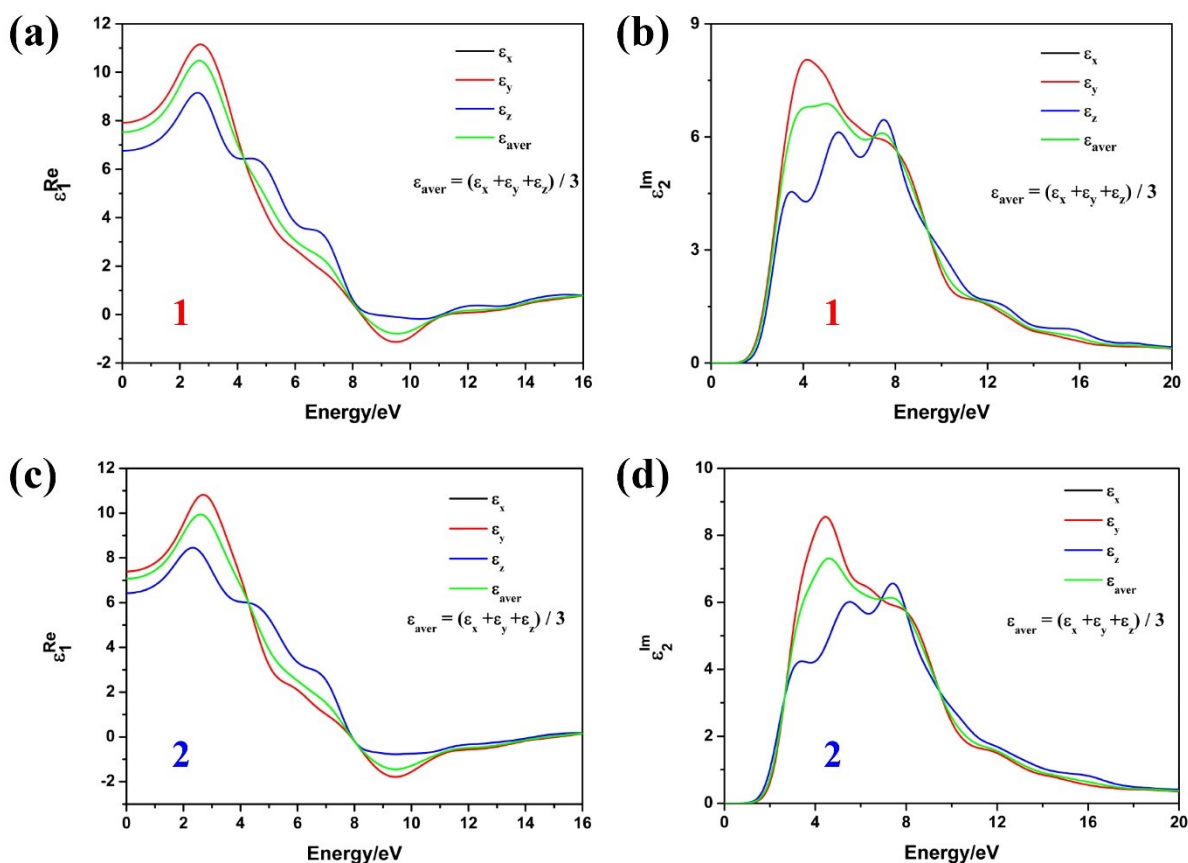**Fig. S6.** FT-IR spectra for **1** and **2**.

Fig. S7. TGA-DSC curves for **1** and **2**.

Fig. S8. The calculated real parts (a and b) and imaginary parts (b and d) of optical dielectric functions for **1** and **2**.
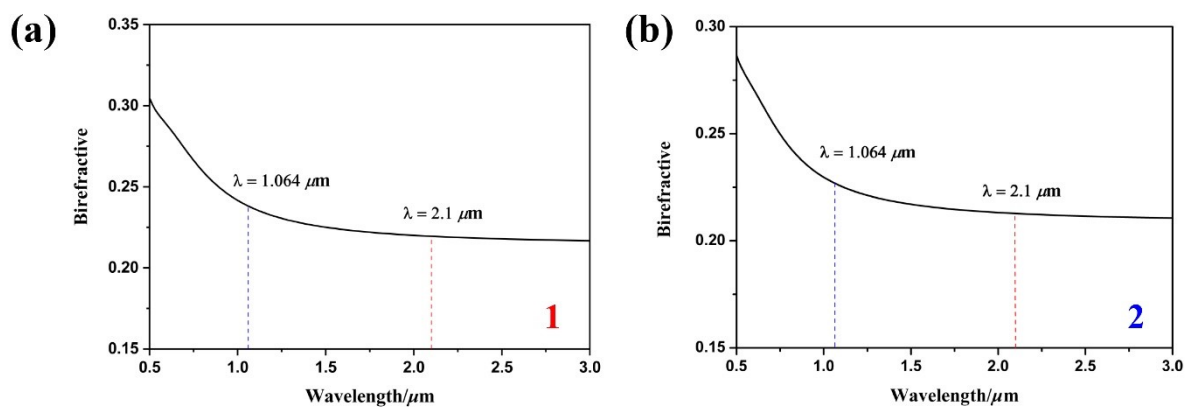
Fig. S9. The frequency-dependent birefringence *Δ*n of (a) **1** and (b) **2**.
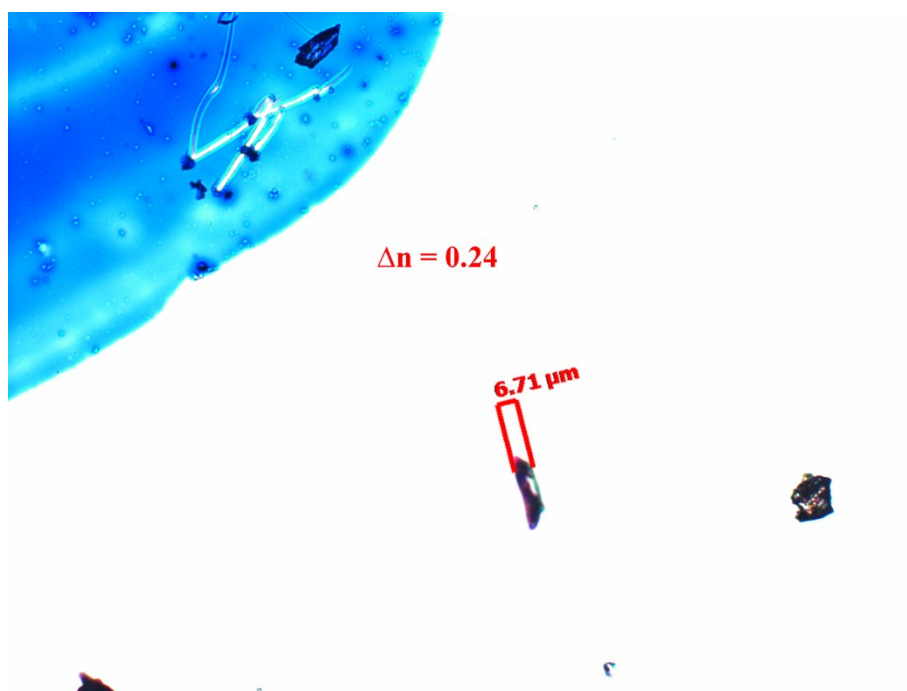

Fig. S10. Photograph of **2** for the birefringence measurement.

REFERENCES

1.   Y. Yang, B. B. Zhang, X. W. Wu and K. Wu, A Series of M_3PS_4 (M = Ag, Cu and Ag/Cu) Thiophosphates with Diamond-Like Structures Exhibiting Large Second Harmonic Generation Responses and Moderate Ion Conductivities, *Dalton Trans.*, 2021, **50**, 4129–4132.

2.   X. Huang, S. H. Yang, X. H. Li, W. L. Liu and S. P. Guo, $Eu_2P_2S_6$: The First Rare-Earth Chalcogenophosphate Exhibiting Large Second-Harmonic Generation Response and High Laser-Induced Damage Threshold, *Angew. Chem. Int. Ed.*, 2022, e202206791.

3.   B. H. Ji, A. Sarkar, K. Wu, A. Swindle and J. Wang, $A_2P_2S_6$ (A = Ba and Pb): A Good Platform to Study the Polymorph Effect and Lone Pair Effect to Form an Acentric Structure, *Dalton Trans.*, 2022, **51**, 4522–4531.

4.   Z. Li, X. X. Jiang, M. L. Zhou, Y. W. Guo, X. Y. Luo, Y. C. Wu, Z. S. Lin and J. Y. Yao, $Zn_3P_2S_8$: A Promising Infrared Nonlinear-Optical Material with Excellent Overall Properties, *Inorg. Chem.*, 2018, **57**, 10503–10506.

5.   W. H. Xing, F. Liang, C. L. Tang, E. Uykur, Z. S. Lin, J. Y. Yao, W. L. Yin and B. Kang, Highly Distorted $[HgS_4]$ Motif-Driven Structural Symmetry Degradation and Strengthened Second-Harmonic Generation Response in the Defect Diamond-Like Chalcogenide $Hg_3P_2S_8$, *ACS. Appl. Mater. Interfaces*, 2021, **13**, 37331–37338.

6.   Z. H. Shi, M. Yang, W. D. Yao, W. L. Liu and S. P. Guo, $SnPQ_3$ (Q = S, Se, S/Se): A Series of Lone-Pair Cationic Chalcogenophosphates Exhibiting Balanced NLO Activity Originating from SnQ_8 Units, *Inorg. Chem.*, 2021, **60**, 14390–14398.

7.   M. L. Zhou, L. Kang, J. Y. Yao, Z. S. Lin, Y. C. Wu and C. T. Chen, Midinfrared Nonlinear Optical Thiophosphates from $LiZnPS_4$ to $AgZnPS_4$: A Combined Experimental and Theoretical Study, *Inorg. Chem.*, 2016, **55**, 3724–3726.

8.   Z. Li, S. Z. Zhang, Z. W. Huang, L. D. Zhao, E. Uykur, W. H. Xing, Z. S. Lin, J. Y. Yao and Y. C. Wu, Molecular Construction from $AgGaS_2$ to $CuZnPS_4$: Defect-Induced Second Harmonic Generation Enhancement and Cosubstitution-Driven Band Gap Enlargement, *Chem. Mater.*, 2020, **32**, 3288–3296.

9. B. J. Song, Z. J. Ma, B. X. Li, X. T. Wu, H. Lin and Q. L. Zhu, Structural Modulation from Cu_3PS_4 to $Cu_5Zn_{0.5}P_2S_8$: Single-Site Aliovalent-Substitution-Driven Second-Harmonic-Generation Enhancement, *Inorg. Chem.*, 2021, **60**, 4357–4361.

10. W. H. Xing, N. Z. Wang, C. L. Tang, C. X. Li, Z. S. Lin, J. Y. Yao, W. L. Yin and B. Kang, From $AgGaS_2$ to $AgHgPS_4$: Vacancy Defects and Highly Distorted HgS_4 Tetrahedra Double-Induced Remarkable Second-Harmonic Generation Response, *J. Mater. Chem. C*, 2021, **9**, 1062–1068.

11. M. Y. Li, Z. Ma, B. Li, X. T. Wu, H. Lin and Q. L. Zhu, $HgCuPS_4$: An Exceptional Infrared Nonlinear Optical Material with Defect Diamond-like Structure, *Chem. Mater.*, 2020, **32**, 4331–4339.

12. W. H. Xing, C. L. Tang, P. F. Gong, J. Y. Wu, Z. S. Lin, J. Y. Yao, W. L. Yin and B. Kang, Investigation into Structural Variation from 3D to 1D and Strong Second Harmonic Generation of the $AHgPS_4$ (A^+ = Na^+, K^+, Rb^+, Cs^+) Family, *Inorg. Chem.*, 2021, **60**, 18370–18378.

13. Y. Wang, Y. Q. Fang, Y. Z. Cao and F. Q. Huang, Two Nonlinear Optical Thiophosphates $Cu_5Hg_{0.5}P_2S_8$ and $AgHg_3PS_6$ Activated by Their Tetrahedra-Stacking Architecture, *Inorg. Chem.*, 2022, **61**, 1620–1626.

14. Y. H. Fan, X. M. Jiang, B. W. Liu, S. F. Li, W. H. Guo, H. Y. Zeng, G. C. Guo and J. S. Huang, Phase Transition and Second Harmonic Generation in Thiophosphates $Ag_2Cd(P_2S_6)$ and $AgCd_3(PS_4)S_2$ Containing Two Second-Order Jahn–Teller Distorted Cations, *Inorg. Chem.*, 2017, **56**, 114–124.

15. Z. Li, S. Z. Zhang, W. H. Xing, Y. W. Guo, C. X. Li, Z. S. Lin, J. Y. Yao and Y. C. Wu, Mixed-Metal Thiophosphate $CuCd_3PS_6$: An Infrared Nonlinear Optical Material Activated by Its Three-in-One Tetrahedra-Stacking Architecture, *J. Mater. Chem. C*, 2020, **8**, 5020–5024.

16. J. H. Feng, C. L. Hu, B. X. Li and J. G. Mao, $LiGa_2PS_6$ and $LiCd_3PS_6$: Molecular Designs of Two New Mid-Infrared Nonlinear Optical Materials, *Chem. Mater.*, 2018, **30**, 3901–3908.

17. J. H. Feng, C. L. Hu, X. Xu, B. X. Li, M. J. Zhang and J. G. Mao, $AgGa_2PS_6$: A New Mid-Infrared Nonlinear Optical Material with a High Laser Damage Threshold and a Large Second Harmonic Generation Response, *Chem. - Eur. J.*, 2017, **23**, 10978–10982.

18. V. Nguyen, B. H. Ji, K. Wu, B. B. Zhang and J. Wang, Unprecedented Mid-Infrared Nonlinear Optical Materials Achieved by Crystal Structure Engineering, a Case Study of $(KX)P_2S_6$ (X = Sb, Bi, Ba), *Chem. Sci.*, 2022, **13**, 2640–2648.

19. M. M. Chen, S. H. Zhou, W. B. Wei, M. Y. Ran, B. X. Li, X. T. Wu, H. Lin and Q. L. Zhu, $RbBiP_2S_6$: A Promising IR Nonlinear Optical Material with a Giant Second-Harmonic Generation Response Designed by Aliovalent Substitution, *ACS Mater. Lett.*, 2022, **4**, 1264–1269